Observed winter salinity fields in the surface layer of the Arctic Ocean and statistical approaches to predicting large-scale anomalies and patterns

Ekaterina A. CHERNIAVSKAIA,[1] Ivan SUDAKOV,[2] Kenneth M. GOLDEN,[3] Courtenay STRONG,[4] Leonid A. TIMOKHOV[1]

[1]*Department of Oceanography, Arctic and Antarctic Research Institute, Bering str. 38, St. Petersburg, 199397, Russia*
[2]*Department of Physics, University of Dayton, 300 College Park, SC 101B, Dayton, OH 45469-2314, USA.*
E-mail: isudakov1@udayton.edu
[3]*Department of Mathematics, University of Utah, 155 S 1400 E, Room 233, Salt Lake City, UT 84112-0090, USA*
[4]*Department of Atmospheric Sciences, University of Utah, 135 S 1460 E, Room 819, Salt Lake City, UT 84112-0090, USA*

ABSTRACT. Significant salinity anomalies have been observed in the Arctic Ocean surface layer during the last decade. Our study is based on an extensive gridded dataset of winter salinity in the upper 50 m layer of the Arctic Ocean for the periods 1950–1993 and 2007–2012, obtained from ∼20 000 profiles. We investigate the interannual variability of the salinity fields, identify predominant patterns of anomalous behavior and leading modes of variability, and develop a statistical model for the prediction of surface-layer salinity. The statistical model is based on linear regression equations linking the principal components of surface-layer salinity obtained through empirical orthogonal function decomposition with environmental factors, such as atmospheric circulation, river runoff, ice processes and water exchange with neighboring oceans. Using this model, we obtain prognostic fields of the surface-layer salinity for the winter period 2013–2014. The prognostic fields generated by the model show tendencies of surface-layer salinification, which were also observed in previous years. Although the used data are proprietary and have gaps, they provide the most spatiotemporally detailed observational resource for studying multidecadal variations in basin-wide Arctic salinity. Thus, there is community value in the identification, dissemination and modeling of the principal modes of variability in this salinity record.

KEYWORDS: atmosphere/ice/ocean interactions, climate change, polar and subpolar oceans

INTRODUCTION

The Arctic Ocean is very sensitive to changing environmental conditions. Its surface layer is a key component of the Arctic climate system, which serves as the dynamic and thermodynamic link between the atmosphere and the underlying waters (Carmack, 2000). Thermohaline characteristics of the surface layer are markedly influenced by atmospheric and sea-ice processes, and wind and buoyancy forcing on this important layer ultimately impact the entire upper ocean (Cronin and Sprintall, 2009). The rejection of salt during sea-ice formation strongly impacts upper ocean salinity, so that the stability and development of the ice cover are closely associated with the thermohaline properties of the upper ocean, such as the depth of the mixed layer and halocline. In this context, the Arctic Ocean surface layer is a critical indicator of climate change (Toole and others, 2010).

Here, salinity is chosen as the main characteristic of thermohaline structure variations of the Arctic Ocean surface layer because, at high latitudes, it mainly determines the density structure (Weyl, 1968; Morison and Smith, 1981; Walin, 1985). The thermohaline structure of the Arctic Ocean surface layer has undergone significant changes in recent years (Macdonald and others, 2005). Of particular interest is the great salinification of the surface layer of the Eurasian and Makarov Basins in the early 1990s – a phenomenon unprecedented in the record back to 1950 (Fig. 1). One hypothesis for this is that the increase of Arctic atmospheric cyclone activity in the 1990s led to a large change in the

salinity in the Eurasian Basin through changes in river inflow, and increased brine formation due to changes in Arctic sea-ice formation (Dickson, 1999; Polyakov and others, 2008). The other reason for salinification is the influence of Atlantic waters (AW), which by 2007 became warmer by ∼0.24°C than they were in the 1990s. Observations show that increases in Arctic Ocean salinity have accompanied this warming as it was associated with significant shoaling of the upper AW boundary and weakening of the upper ocean stratification in the Eurasian Basin as well. That led to facilitated exchange between AW and the upper layer (Polyakov and others, 2010). However, recent observations also show that the upper ocean of the Eurasian Basin was appreciably fresher in 2010 than it was in 2007 and 2008 (Timmermans and others, 2011).

In addition, there have been observations of surface-layer freshening in the Canada Basin. Jackson and others (2012) emphasized that processes related to warming and freshening the surface layer in this region had transformed the water mass structure of the upper 100 m. With these changes, energy absorbed during summer can enter the deepening winter mixed layer and melt sea ice (Timmermans, 2015).

The problem of variability of Arctic Ocean salinity is challenging from a theoretical perspective. For example, Lique and others (2009) performed an analysis of the variability of Arctic fresh water content informed by a global ocean/sea-ice model. The authors uncovered important spatial
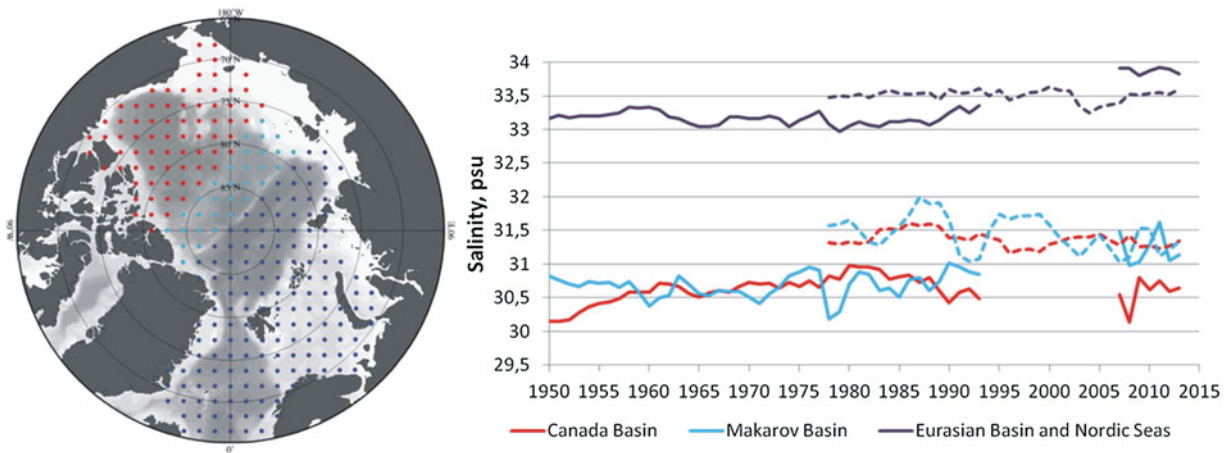
Fig. 1. Temporal changes in salinity averaged over the depth range 5–50 m. Dashed curves show salinities from PIOMAS data. Grids with spatial resolution 200×200 km were obtained as the result of interpolation and reconstruction (see section 'Field reconstruction and interpolation') of bottled and CTD data.

contrasts in the influence of velocity and salinity fluctuations on ocean fresh water transport variability. They conclude that variations of salinity (controlling part of the Fram fresh water export) arise from the sea-ice formation and melting north of Greenland. Jahn and others (2012) compared simulations from ten global ocean–sea-ice models of Arctic fresh water, and concluded that improved simulations of salinity variability are required to advance understanding of liquid fresh water export.

Improving the representation of the salinity distribution is crucial. However, inclusion, representation and parametrization of a number of processes is required (Steele and others, 2001; Komuro, 2014). For example, in many global ocean–sea-ice models, salt rejection in the first level of the ocean model during ice formation leads to an unrealistic salt distribution in the mixed layer and below (Nguyen and others, 2009).

The transfer of fresh water and sea ice from the Arctic Ocean to the North Atlantic are significant components of global ocean circulation (Haak and others, 2003; Gelderloos and others, 2012). Thus, the investigation of the variability of the surface layer (the upper 50 m) can make a significant contribution to understanding ocean-climate feedback. In particular, abrupt changes in surface-layer salinity may lead to critical transitions in the patterns of global ocean circulation, such as convection shut downs and climate disruptions (Hall and Stouffer, 2001; Gelderloos and others, 2012). A robust conceptual statistical model may help to describe the features of anomalies in salinification of the Arctic Ocean, which are key players in the formation of surface-layer salinity patterns. In this case, investigation of the structure of patterns and quality of anomalies leads to a better understanding of possible critical transitions in the patterns of global ocean circulation. Variations of Arctic Ocean surface-layer salinity have complex spatial and temporal structures, which are affected by many external factors. Our aim is to distinguish the most significant factors that led to recent changes in surface-layer salinity patterns.

Here, we present a statistical model for Arctic Ocean salinity fields based on multiple linear regression analysis, which builds on ideas presented in prior studies (e.g., Timokhov and others, 2012). This statistical model of variability of Arctic Ocean winter salinity in the 5–50 m layer is used as a method of reconstruction of observed winter

salinity fields presented in Pokrovsky and Timokhov (2002). The model is based on an empirical orthogonal function (EOF) decomposition of the salinity data (e.g., Hannachi and others, 2007), and a multiple correlation analysis of the time series associated with the first three leading modes, or principal components (PCs); see Appendix Box 1 for a schematic diagram of the model. The contribution of atmospheric factors and hydrological processes in the spatial distribution of surface-layer salinity was interpreted by determining the structure of the multiple correlation equations. The variability patterns and relationships identified through the statistical analysis and modeling inform a conceptual model for principal drivers of Arctic salinity.

METHODS

Data set

This study is based on a collection of more than 9800 instantaneous temperature and salinity profiles, with data available at the standard levels (5, 10, 25, 50, 75, 100, 150, 200, 250, 300, 400, 500, 750, 1000 and so on every 500 m), collected between 1950 and 1993. The data were obtained from the Russian Arctic and Antarctic Research Institute (AARI) database, which was also used in the creation of the Joint US–Russian Atlas of the Arctic Ocean for winter (Timokhov and Tanis, 1997). The AARI database was first introduced by Lebedev and others (2008). This is complemented by the data made available over the period 2007–2012 from the expeditions of the International Polar Year (IPY) and afterward, which consist of Conductivity Temperature Depth (CTD) and eXpendable Conductivity Temperature Depth (XCTD) data, as well as data from the Ice-Tethered Profiler (ITP)-buoys (more than 14 600 stations in total). The average vertical resolution of all these profiles was 1 m. In areas where observations were missing, temperature and salinity data were reconstructed in a regular grid for the period 1950–1989 as detailed in the next subsection. The time period of 1994–2006 was not included in the analysis as there are too few data to construct reliable gridding fields. Thus, the working database is represented by grids with 200 km horizontal spacing, covering the deep part of the Arctic Ocean (with depths of more than 50 m). According to Treshnikov (1959), Rudels and others (1996, 2004) and

Korhonen and others (2013), the average thickness of the Arctic Ocean mixed layer for the winter season is ~50 m. A description of the data sources for other physical parameters, used as predictors for the statistical model, can be found in Table 1.

The database used in this study belongs to the Oceanography Department of the Arctic and Antarctic Research Institute and it is not freely available. To mitigate the related issues, we provide additional data description. Table A1 in the Appendix contains a list of the expeditions and number of stations that were used for reconstruction and gridding of salinity fields. Figure A1 shows the overall observation density and the year associated with each observation. The data exhibit a spatiotemporal non-uniformity that is undesirable but expected given the logistical challenges associated with recovering long-term observations of Arctic salinity. While this dataset has gaps and is proprietary, we believe it provides one of the most spatiotemporally detailed observational resources for studying multidecadal variations in basin-wide Arctic salinity. This manuscript is motivated by the potential to advance understanding through identification, dissemination and modeling of the principal modes of variability in these long-term salinity observations.

Gridded fields of surface winter salinity were compared with fields from the Pan-Arctic Ice-Ocean Modeling and Assimilation System (PIOMAS; Zhang and Rothrock, 2003; Lindsay and Zhang, 2006) for their overlapping period 1978–1993 (dashed curves, Fig. 1). PIOMAS is a coupled ice-ocean model which uses data assimilation methods for ice concentration and ice velocity. Forced by atmospheric observations, its output is available for 1978 to near present and is widely used as a reference for Arctic variables with limited long-term observations including salinity and sea-ice thickness. Maps of long-term means for both datasets are similar (Figs 2a and A2a), with a correlation coefficient of 0.88. Nevertheless, PIOMAS data generally provide higher salinity values for the Amerasian Basin (Canada Basin together with Makarov Basin) for the overlapping period (Fig. 1). The associated variance maps are also significantly correlated with each other (correlation coefficient $R = 0.36$; statistical significance level $p = 0.05$) but exhibit some salient differences (Fig. A3). In particular, a high variance zone along the Lomonosov Ridge is prominent in the AARI dataset, but is absent in PIOMAS data. PIOMAS instead features several centers of high variance along the shelf.

To test for artifacts from the data gaps and the interpolation procedure (reviewed in the next subsection), we make several comparisons across methods and to independent datasets in the subsections to follow. For example, we also performed the EOF analysis with and without the additional 2007–2012 period, and report only modest change to the resulting modes of variability (section 'Decomposition of surface-layer salinity fields by EOF'). In section 'Decomposition of surface-layer salinity fields by EOF', we also compare EOFs from the AARI data to those from PIOMAS.

Field reconstruction and interpolation

To provide temporal and spatial continuity, we have unified existing datasets using reconstruction and gridding. The

Table 1. Predictors used for the approximation of PCs

| Physical processes and its notation	Physical value	Description	Data sources (references and the web sources)
Arctic oscillation index (AO)	First EOF-mode of sea-level pressure north of 60N latitude	When the AO index is positive, surface pressure is low in the polar region. When the AO index is negative, there tends to be high pressure in the polar region.	Thompson and Wallace (1998). NOAA Center for Weather and Climate Prediction (NCWCP) http://www.esrl.noaa.gov/psd/data/gridded/
Arctic dipole anomaly index (AD)	Second EOF-mode of sea-level pressure north of 60N latitude	When the AD index is positive, sea-level pressure has a positive anomaly over the Canadian Archipelago and a negative anomaly over the Barents Sea. When the AD index is negative, SLP anomalies show an opposite scenario, with the center of negative SLP anomalies over the Nordic seas (Wu and others, 2006; Wang and others, 2009; Overland and Wang, 2010).	Overland and Wang (2010). NOAA Center for Weather and Climate Prediction (NCWCP) http://www.esrl.noaa.gov/psd/data/gridded/
Atlantic multi decadal oscillation index (AMO)	Variations of sea surface temperature in the North Atlantic Ocean	Index has cool and warm phases that may last for 20–40 years at a time and a difference of ~0.5°C. It reflects changes of sea surface temperature in the Atlantic Ocean between the equator and Greenland. It was used as a substitute for processes of water exchange with the Atlantic Ocean.	Enfield and others (2001). ESRL Physical Sciences Division (PSD) http://www.esrl.noaa.gov/psd/data/timeseries/AMO/
The Pacific decadal oscillation index (PDO)	North Pacific sea surface temperature variability	When the PDO index is positive, the west Pacific becomes cool and part of the eastern ocean warms. When the PDO index is negative, the opposite pattern occurs. It shifts phases on at least the interdecadal timescale, usually ~20–30 years.	Trenberth and Hurrell (1994). Joint Institute for the Study of the Atmosphere and Ocean (JISAO)http://jisao.washington.edu/pdo/
River runoff (RIV)	Water flows	Average annual runoff of the main Siberian rivers. It was used as total runoff in the Kara Sea (K), Laptev Sea (L), East-Siberian Sea (E) and Chukchi Sea (C).	Timokhov and Tanis (1997). Joint US–Russian Atlas of the Arctic Ocean http://rims.unh.edu/data/station/list.cgi?col=4
Area of open water in Arctic seas (OW)	Area	Total ice-free area in the Kara Sea (K), Laptev Sea (L), East-Siberian Sea (E) and Chukchi Sea (C) in September.	Russian Arctic and Antarctic Research Institute (AARI) http://www.aari.ru/projects/ECIMO/index.php?im=100
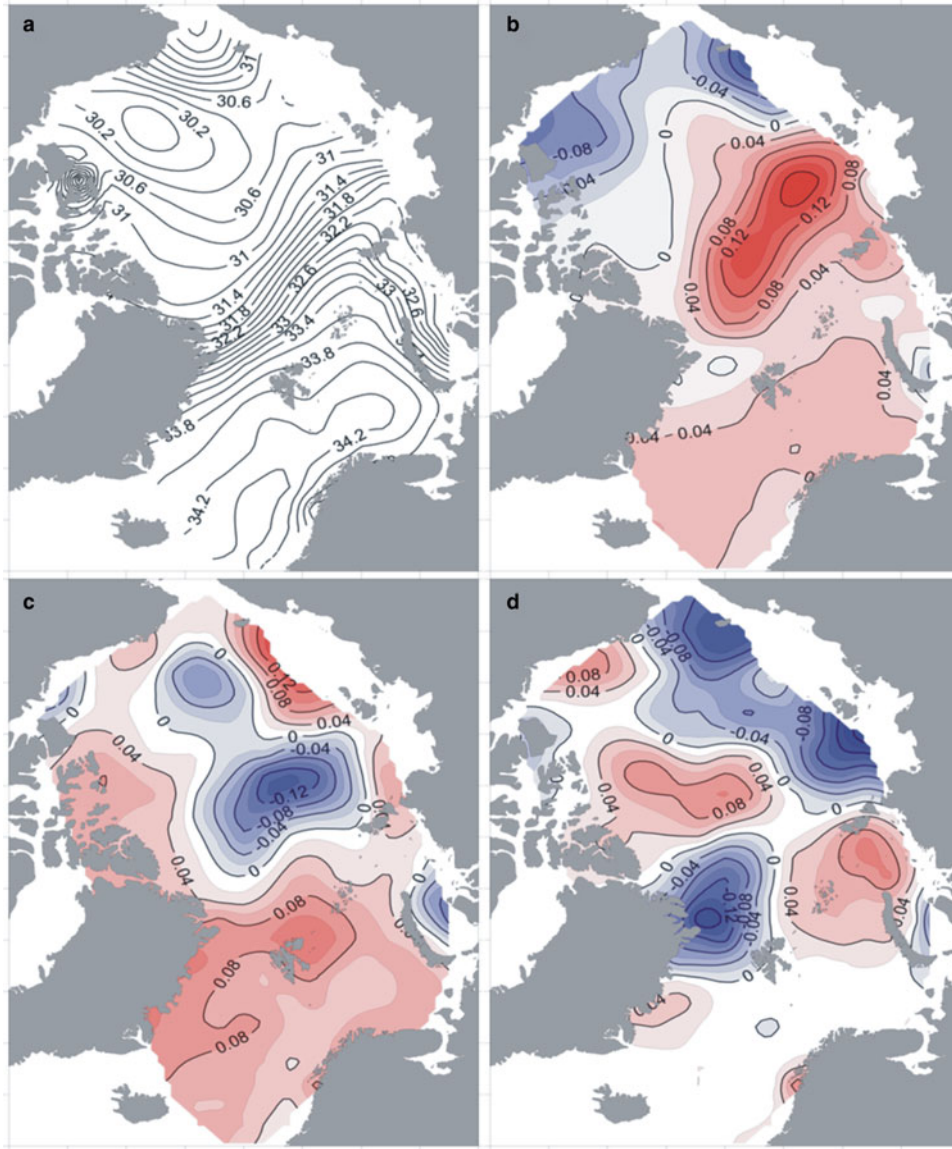
Fig. 2. The average salinity field (a) and first three modes of the average salinity field decomposition for the layer 5–50 m: (b), (c), (d) – first, second and third modes, respectively, for the periods 1950–1993 and 2007–2012.

technique of computing gridded fields for the period from 1950 to 1993 was described by Lebedev and others (2008), and is summarized here.

These techniques are based on the method of ocean field reconstruction, proposed by Pokrovsky and Timokhov (2002). This method, which was used to obtain gridded salinity fields, is given by

$$z_i = z_i^{(r)} + e_i, \quad \langle z_i z_j \rangle = \sigma_{x_i x_j}, \quad \langle z_i e_i \rangle = 0,$$
$$\langle e_i \rangle = 0, \quad \langle e_i e_j \rangle = \delta_{ij} \sigma_e^2 = \sigma_{e_{ij}}^2. \tag{1}$$

Here $z(t, x)$ is the measured value of an oceanographic variable (e.g., temperature or salinity), and is a random function of time t and spatial coordinates x; i and j are the nodes of the irregular data grid; the notation $<\ldots>$ denotes the ensemble average of a value. We can write the observed value of $z(t, x)$ as the sum of a true value $z^{(r)}(t, x)$ of the oceanographic variable and an observational error $e(t, x)$. In addition, we introduce $\sigma_{x_i x_j}$ as a std dev. of spatial coordinates and $\sigma_{e_{ij}}^2$ as a std dev. of errors. We also propose that $z_i^{(r)}$ has spatial

correlations to the oceanographic parameters; that a systematic error is not identified; a std dev. of error (σ_e^2) does exist; and $\delta_{ij} = \begin{cases} 0, & \text{if } i \neq j \\ 1, & \text{if } i = j \end{cases}$ is the Kronecker δ.

Biorthogonal decomposition of the oceanographic variable can help to identify the connections between spatial and temporal distributions within the data:

$$z(t_j, x_i) = \sum_k c_k^j f_k(x_i) + e(t_j, x_i), \tag{2}$$

where $f_k(x_i)$ is the spatial EOF, and c_k^j is the calculated coefficient or so-called k^{th} PC.

As the next step, we approximate the EOF through linear combinations (with coefficients b_{kl}) of convenient analytical functions $P_l(x_i)$ (e.g., polynomials, splines, etc.):

$$f_k(x_i) = \sum_l b_{kl} P_l(x_i). \tag{3}$$

Thus, the modified biorthogonal decomposition can be written as

$$z(t_j,\, x_i) = \sum_k d_l^j P_l(x_i) + e(t_j,\, x_i), \qquad (4)$$

where $d_l^j = \sum b_{kl}\, c_k^j$.

The main goal of this spectral analysis method is to estimate the coefficients of spectral decomposition $\{c_k^j\}$ and $\{b_{kl}\}$, in order to identify dominant modes of behavior. In this case, we rewrite formula (2) in the following matrix form:

$$Z = F \cdot C + e, \qquad (5)$$

where $\cdot$ denotes matrix multiplication.

The matrix F is formed by the values of the EOF, the matrix Z is composed of the totality of the measurement data at the points of the observation net x_i, and the matrix e is filled out by observational error values.

The system of linear equations (5) with respect to the unknown coefficients c_k^j can be solved on the basis of the a priori statistical information (1) with the use of the standard estimation of the least squares method. A formula for the estimation of the matrix of the unknown coefficients C was obtained in (Pokrovsky and Timokhov, 2002), and is written

$$\hat{C} = (F^{\mathrm{T}} \cdot K_e^{-1} \cdot F + K_c^{-1})^{-1} F^{\mathrm{T}} \cdot K_e^{-1} \cdot Z', \qquad (6)$$

where X^{-1} and X^T denote the inverse and transpose of a matrix X, respectively. The covariance matrix of errors of the expansion coefficients K_c is a diagonal matrix composed of eigenvalues of the covariance matrix K_z. Here, the matrices K_z and K_e are covariance matrices of the std dev. of spatial coordinates and the std dev. of errors, respectively.

In order to obtain an estimate of the unknown variables at the nodes of the regular grid $\tilde{x}_i$, it is necessary to interpolate the EOF into the corresponding nodes of the grid and obtain a new matrix $\tilde{F}$ of the EOF, a new matrix $\tilde{C}$ of decomposition coefficients, and new matrix $\tilde{e}$ of observational errors. Using the matrix $\tilde{F}$ obtained in this way and the estimates of the coefficients $\hat{C}$ from formula (6), from the matrix relationship

$$\tilde{Z} = \tilde{F} \cdot \tilde{C} + \tilde{e}, \qquad (7)$$

we obtain an estimate of the unknown parameters at the nodes of a regular grid. Simultaneously with the salinity fields in the nodes of a regular grid, we can also calculate the covariance matrices of the errors of estimations obtained from the following equations:

$$K_{\hat{C}} = \left(I + \left(K_c \cdot \left(\tilde{F}^{\mathrm{T}} \cdot \tilde{K}_e^{-1} \cdot \tilde{F} \right) \right) \right)^{-1} \cdot K_c,$$

$$K_{\hat{Z}} = \tilde{F} \cdot K_z \cdot \tilde{F}^{\mathrm{T}}, \qquad (8)$$

where I is the identity matrix and $\tilde{K}_e^{-1}$ is the covariance matrix of the observation error expanded over the regular grid x_i.

This approach is a combination of singular value decomposition and statistical regularization. These coefficients (modes) can be linked to the real physical processes that influence salinity as presented in section 'Statistical approach'. Preparation of the average salinity field data for 2007–2012 consisted of several stages as detailed in the Appendix. First, we checked the data for random errors. Then, we used linear interpolation and assimilated the real

plane with the field data through the virtual plane of data. Next, we constructed an interpolation via a grid of nodes (separately for each plane). The gaps in the data for uncovered sites were filled with climatic values from the Joint US–Russian Atlas of the Arctic Ocean (Timokhov and Tanis, 1997). Using an older climatology to fill in recent (2007–2012) salinity fields is appropriate here as the areas where the most significant changes are observed, i.e., Canadian and Eurasian Basins, have sufficient data coverage to lessen concerns about potential inaccuracies (Fig. A1).

Statistical approach

Here we describe the approaches to data analysis which were used for physical interpretation of our statistical model. Polyakov and others (2010), Rabe and others (2011) and Morison and others (2012) have emphasized that the thermohaline structure of the surface layer has undergone significant change over the last decade. However, there is still room for discussion on what physical processes led to these changes or what the future trends may be.

The analysis of the variability of the surface layer (including salinity fields) of the Arctic Ocean may be based on a decomposition using EOFs. This approach is useful in our case because decomposition by EOF analysis gives modes (spatial patterns) and PC time series, which allow us to divide the variability into spatial and temporal components. Each mode describes a certain fraction of the total variance of the initial data, and the EOFs are conventionally ordered so that the first EOF explains the most variance and subsequent EOFs explain progressively less variance (Hannachi and others, 2007). The first three modes describe more than half the variance of the analyzed fields as further detailed below, which allows significant compressing of the information contained in the original data (Hannachi and others, 2007; Borzelli and Ligi, 1998). The EOF decomposition was carried out for the average salinity fields for the layer 5–50 m, yielding PCs for the periods of 1950–1993 and 2007–2012.

Multiple linear regression was used to model the PC time series to identify predictors that determined variability of the salinity fields. The regression equations can give projections of future changes because the predictors lead the salinity field by various temporal lags. The statistical model is characterized by a system of linear regression equations constructed for the first three PCs. The candidate predictors were as follows: atmospheric circulation indices (Arctic oscillation (AO) and Arctic dipole (AD) indices; see Table 1) calculated for winter (October–March to cover the period of active ice formation) and summer (July–September to cover the period of active ice melting), river runoff, the area of the ice-free surface in Arctic seas in September and water exchange with the Pacific and Atlantic Oceans. For the latter two water exchanges, we used the Pacific decadal oscillation (PDO) and Atlantic multidecadal oscillation (AMO) indices as respective proxies because of their influence on the temperature and salinity of water, which is entering through the Bering Strait and the Faeroe-Shetland Strait to the Arctic Ocean (Zhang and others, 2010; Dima and Lohmann, 2007). Atmospheric indices were averaged by different time periods within indicated winter and summer seasons. The optimal periods of averaging for a particular index were chosen on the basis of maximal correlations with PCs.

RESULTS

Decomposition of surface-layer salinity fields by EOF

As a result of EOF decomposition of the salinity fields for the 5–50 m layer, we obtained two sets of modes and PCs – one for the period of 1950–1993 (series 1) and one for the same period adding the years 2007–2012 (series 2). North's rule of thumb states the following: if the sampling error in an eigenvalue is comparable to the distance to a neighboring eigenvalue, then the sampling error of the EOF will be comparable to the size of the neighboring EOF (North and others, 1982). Based on this rule, the first three modes were accepted for further analysis as physically significant. The first three modes obtained by the decomposition of series 1 describe more than 55% of the total dispersion of the initial fields. The first three modes of series 2 describe more than 61% of the total dispersion. Nevertheless, the first modes for both decompositions have very similar shapes. The only differences are a more distinct dipole structure between the Canada Basin and Eurasian Basin, and positive EOF loading (instead of negative in the first mode of series 2) over much of the Nordic seas that appears in the first mode of series 2. As the Nordic seas region is the pathway of AW in the Arctic Basin (Karcher and others, 2007), we assume that the change of sign of EOF values is associated with increased temperature and salinity of AW inflow and subsequent salinification of the Eurasian Basin (Polyakov and others, 2010; Beszczynska-Möller and others, 2012). Thus, the modes obtained by decomposition in series 1 cannot take into account the essential features of the distribution of surface-layer salinity fields associated with the salinification of the Eurasian Basin. Therefore, for further analysis we used the PCs and modes obtained upon decomposition in series 2 (Fig. 2).

As a point of comparison for these EOFs, Appendix Fig. A2 presents a similar EOF analysis using model output from the PIOMAS. The spatial pattern of PIOMAS mean salinity (Fig. A2a) reasonably resembles the pattern shown for our data in Figure 2a. EOFs of PIOMAS salinity after detrending (Figs A2b–d) repeat the main features of corresponding results in Figure 2b–d, despite incomplete overlap over the analysis periods. In particular, for both datasets, the leading EOF for salinity features a prominent dipole between the Canada Basin and Eurasian Basin (Figs 2b and A2b). However, the leading EOF of PIOMAS salinity has a more patchy structure. In particular, there are negative centers of action situated along the Siberian shelf break, along with freshened areas (Fig. A2a) that are not as clearly pronounced in the AARI salinity data (Fig. 2a). The second EOF of salinity features a negative center of action elongated along the Lomonosov Ridge surrounded by positive loading strongest along Siberian shelf (Figs 2c and A2c). Less agreement is seen for the third EOF (Figs 2d and A2d), which is perhaps unsurprising in moving toward modes accounting for less variance.

The linear regression equation for the PCs

We present here a statistical model of interannual variability of Arctic Ocean surface-layer salinity. This research builds on already established approaches used by Pokrovsky and Timokhov (2002), specifically their reconstruction of salinity fields applying modified EOF methods.

We suggest some additions to improve on the ideas presented in previous research by Timokhov and others (2012). For example, the analysis presented is based on a dataset updated for the period 2007–2012, which is important for understanding the physical processes during the dramatic recent changes in Arctic sea ice. The area under consideration was extended and includes the Nordic seas and part of the Siberian shelf with depths of more than 50 m. This expanded domain allowed consideration of the areas strongly influenced by river runoff and ice processes, and makes visible their effects on the structure of the EOFs. Also, in contrast to our previously published research (Timokhov and others, 2012), we do not use the previous values of the PCs (history) as predictors for linear regression, which simplifies the physical interpretation of the equations obtained.

A set of external factors having the most correlation with salinity values (the predictors as described in section 'Statistical approach') have been defined based on the results of correlation analysis. As a result of linear regression analysis, we obtained empirical equations for the first three PCs (see Table A2 in Appendix). The structure of these equations can be explained through the sets of factors that simulate the effects of both atmospheric and hydrological processes.

Thus, the predictors used can be divided into two groups. The first group includes atmospheric circulation indices and reflects the influence of atmospheric processes. The second group corresponds to hydrological processes: river runoff into Arctic seas, inflows through the Bering Strait and the Faeroe-Shetland Strait, which were characterized by the PDO and AMO indices, and the areas of open water in the Arctic seas in September. Predictors were included in the equations with different time shifts (lags). The value of the time shift was 1–10 years and was chosen to maximize correlations of predictors with the PCs as noted above.

The contribution of each group to the explained variance in PC_1 through PC_3 can be calculated based on the magnitude and sign of the regression coefficients of corresponding predictors included in that particular group. In this case, hydrological processes have a dominant contribution to the explained variance of all PCs (from 86 to 61%). Atmospheric factors (i.e., AO and AD) contribute from 14 to 39%.

DISCUSSION AND SUMMARY

The first mode of the surface-layer salinity decomposition (EOF_1) displays an out-of-phase relationship between salinity anomalies in the Canada and Eurasian Basins (which includes the Nansen and Amundsen Basins) and Makarov Basin (Fig. 2b).

In the late 1980s, as a consequence of surface air temperature rising, the atmospheric circulation regime in the Arctic began to change (Steele and Boyd, 1998; Proshutinsky and others, 2009; Morison and others, 2012). Degradation of the Arctic anticyclone, shifting of the pressure pattern in the Beaufort Sea counterclockwise from the 1979–1992 pattern (Morison and others, 2000) and strengthening of the dipole pressure pattern (Overland and others, 2010) were observed. According to Wang and others (2009), large values of the AD indices (higher than 0.6 std dev.) could be a primary reason for the historical record lows of sea-ice extent in the summers of 1995, 1999, 2002, 2005 and 2007. In addition, in the late 1980s, the inflow of warm

and highly saline AW into the Arctic Basin increased (Morison and others, 2000; Polyakov and others, 2010). Observed shoaling of the AW upper boundary, together with a decrease of static stability in the halocline layer, led to an increase in upper layer temperature and salinity in the Eurasian Basin (Polyakov and others, 2010). At the beginning of this century, the heat flux through the Bering Strait to the Chukchi Sea increased (Woodgate and others, 2010). Comparatively warm and fresh (salinity range $31 < S < 32$) summer Pacific waters, due to their low density, were able to inject heat close to the ocean surface (Stigebrandt, 1984) and enhance ice melting in the Canada Basin (Shimada and others, 2006) which led to decreasing surface-layer salinity in this region.

These observations allow us to suggest that salinity differences between the Canada Basin and Eurasian Basin, which became more pronounced in recent years (Fig. 1), are the consequence of these processes. Our suggestion is supported by the regression equation for PC_1 (Table A2) from which we see that PC_1 is a function of AMO, PDO, open water area in the East Siberian and Chukchi seas (that can be considered as an indirect indicator of fresh water inflow from these seas to the Arctic) and summer AO index. The time lags must be related with the time that it takes for Atlantic and Pacific waters to reach the Arctic Basins and become involved in associated circulation.

According to Karcher and others (2002), travel time for the propagation of anomalies in AW is 5–10 years from the Nordic Seas to the Eurasian Basin. This is reflected by AMO time lags. Bourgain and Gascard (2012) revealed that the warm signal from the Bering Strait propagated in the interior of the Canada Basin over 4–5 years. A proxy of this process is the PDO. The travel times for the Siberian river water from the river mouths to the shelf edge are estimated to be 2–5 years (Schlosser and others, 1994; Karcher and others, 2002). These time periods are in good agreement with time lags of the statistical model predictors, which may vary from 3 to 10 years (Table A2).

EOF_2 exhibits opposite polarity of salinity anomalies in the central Arctic Ocean and near-slope areas (Fig. 2c). Spectral analysis of the associated PC_2 revealed a 9-year cycle (periodogram is not shown here), which we associate with shifts between cyclonic and anticyclonic circulation regimes (Proshutinsky and Johnson, 1997; Rigor and others, 2002). The regression equation for PC_2 demonstrates its dependence on the summer AO and AD indices. Thus, during an anticyclonic regime of atmospheric circulation, fresh surface waters tend to flow to the center of the Arctic basin and negative salinity anomalies form there. At the same time, along the slopes there is upwelling of AW and positive salinity anomalies occur (Proshutinsky and Johnson, 1997). During a cyclonic circulation regime, reversed momentum forcing should likewise produce positive salinity anomalies in the central Arctic and negative salinity anomalies along the slopes.

The contribution of each predictor in the variability of a particular PC was evaluated as:

$$I = \frac{\sigma_i \cdot \alpha}{\sum (\sigma_i \cdot \alpha)} \cdot 100\%, \qquad (9)$$

where σ_i is the std dev. of the predictor and α is the regression coefficient of the predictor. According to this formula, contributions of the predictors for PC_2 (Table A2) were calculated.

PDO and river runoff from the Laptev, East Siberian and Chukchi Seas make the largest contribution to the variability of PC_2 (33.8 and 26.9%, respectively) with slightly weaker effects from AO and AD (20.5 and 18.9%).

EOF_3 is represented by a field with multicore structure (Fig. 2d). The positive centers of action spread from the Beaufort Sea over the North Pole to the Kara Sea and are surrounded by negative centers of action. This kind of distribution is associated with an AD (Wu and others, 2006). The winter AD index accounts for ∼22% of the variability of PC_3. The most distinct negative cores are located along the shelf of the Laptev and Chukchi Seas and also near Greenland. In our statistical model, associated variations are accounted for by river runoff from the Laptev, East Siberian and Chukchi Seas, the PDO index, and the AMO index, which account for 20, 25.8 and 32.4% of the variability of PC_3, respectively (Table A2).

All predictors included in the regression equations (with particular time lags and averaging periods) are statistically independent, i.e., they are not significantly correlated with each other, except for AMO (-10) and PDO (-3). These indices have a slight positive correlation ($R = 0.33$), but this
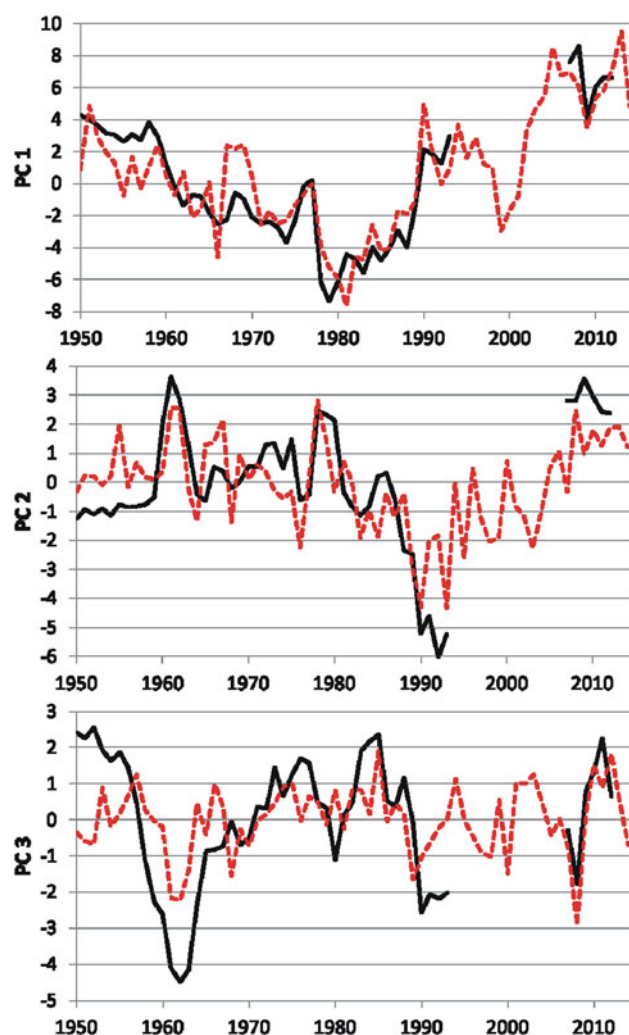

Fig. 3. The actual (black line) principal components and calculated principal components (red dashed line) with the help of the equations of linear regression. Correlation coefficients between the calculated time series of PCs and actual PCs are: $r(PC_1) = 0.88$; $r(PC_2) = 0.73$; $r(PC_3) = 0.55$.
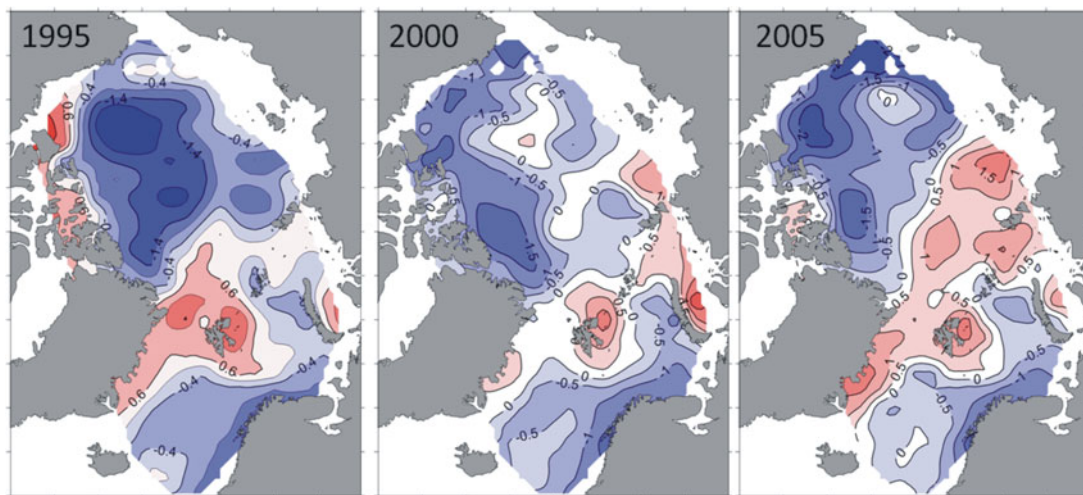
Fig. 4. Maps of differences of salinity fields reconstructed with the statistical model and those from PIOMAS data.

is not a concern because they have different regions of influence and are associated with different proxies.

Time series of PC_{1-3} show a mixture of interannual and quasidecadal oscillations (Fig. 3). Based on the configurations of the EOFs (Fig. 2), the regression equations (Table A2) and results of the spectral analysis of the PCs, we may assume that large-scale surface-layer salinity anomalies (with periods longer than 20 years) are the result of water exchange effects. The shorter period (8–9 years) variations appear to be determined by atmospheric circulation processes. Also, interannual variations occur due to interannual variability of both atmospheric and hydrological processes.

The derived equations in the Appendix (Table A2) describe the first three PCs for the period 1950–2012. Calculated with these equations, the modeled PCs agree well with the values of the PCs directly derived from the decomposition of salinity fields via EOF analysis (Fig. 3).

Theoretically, the salinity fields for 1994–2006 can be reconstructed using this statistical model. We noted above that this period had gaps in observational data. The salinity fields of 1995, 2000 and 2005 were chosen for reconstruction to demonstrate the capabilities of the statistical model. The results were compared with PIOMAS model data. Although reconstructed fields have high significant correlations with the PIOMAS fields (correlation coefficients are 0.84, 0.88 and 0.81), in the Amerasian Basin they show lower salinity values than the PIOMAS data. Differences in this region may reach 2 psu. In the Eurasian Basin, specially over the Lomonosov Ridge, the reconstructed salinity values are higher than the PIOMAS data with differences of up to 1.5 psu (for 2005) (Fig. 4).

We also applied our statistical model to the reconstruction of salinity fields for 2013–2014, extending beyond the data record in order to develop a retrospective forecast (sometimes referred to as a hindcast). As a result, we obtained salinity fields that correspond to the trends observed in recent years. This preserved the freshening in the Canada Basin as well as salinification of the surface layer over the Lomonosov Ridge (compared with average surface-layer salinity for 1961–1990) (Fig. 5). According to our modeled values for 2013–2014, freshened water from the Beaufort Gyre should have moved westward along the Canadian Continental Slope in 2013. There are also negative salinity

anomalies observed in the Arctic seas along the Siberian shelf. These processes were able to freshen the Eurasian Basin slightly so that in 2014 positive salinity anomalies over the Lomonosov Ridge were lower than in 2013. To demonstrate the quality of the forecast, we compared the salinity field for 2013 with the corresponding gridded field of observational data and PIOMAS data (Fig. 5). As we were not able to find enough data in winter 2014 to produce a reliable gridded field, comparison for this year was not conducted. In both cases, the reconstructed values are lower in the Canadian Basin and higher in the Eurasian Basin. However, our results are closer to the observational data than to the PIOMAS data, as differences in the first case are not larger than 0.7 psu (Fig. 5d), and in the second case, they are as large as 2.5 psu (Fig. 5f). In any case, PIOMAS data always show higher salinity values in the Amerasian Basin and lower values in the Eurasian Basin than prognostic or reconstructed fields. Some discrepancies from PIOMAS are expected for at least two reasons. First, PIOMAS salinity fields are simulated values not directly guided by salinity data assimilation. Second, the statistical model we use here is based on a subset of the EOFs and thus does not represent all the observed salinity variance as further discussed below.

This method of salinity reconstruction may suffer from inaccuracies due to the higher frequency variability of the calculated PCs. The model may not reliably generate PCs for short-term time series and does not reflect properly the effect of short-term processes such as seasonal variations of ice melting/formation or river runoff, although the trend in variability of all three PCs is reproduced correctly. Therefore, the model can be used for tracking long-term processes of the structural transformation of salinity fields.

Validation of the model was carried out by calculating an error of reconstruction for the surface-layer salinity fields. The difference between the actual and reconstructed salinity fields (ε) was determined as a percentage by the following formula:

$$\varepsilon = (\sigma(S_f - S_c)/\sigma(S_f)) \cdot 100\%, \qquad (10)$$

where σ is the std dev., S_f is the actual salinity and S_c is the calculated salinity.

Twelve surface-layer salinity fields from the time series under consideration (fields for the years 1950, 1955, 1960,
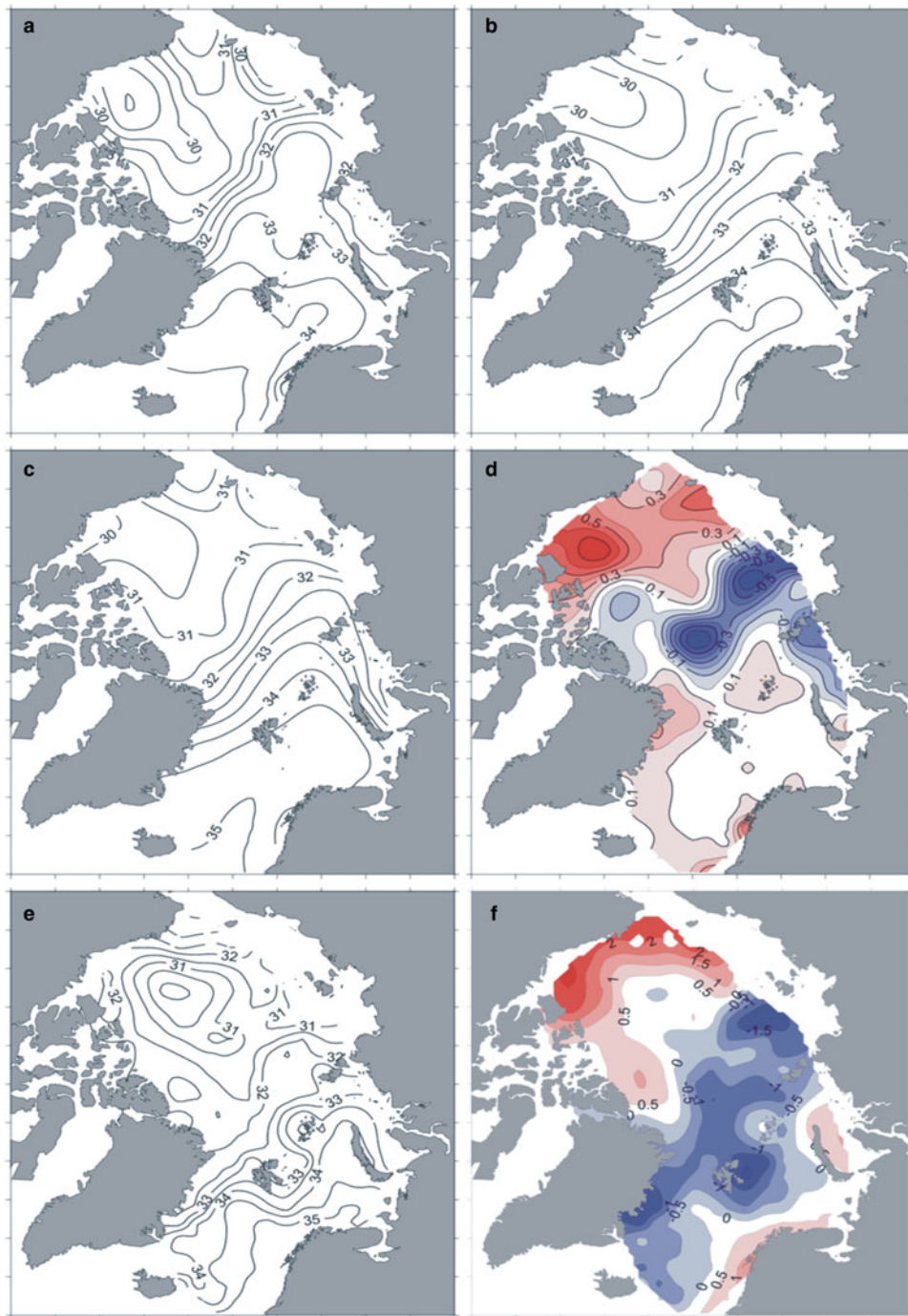
Fig. 5. Reconstructed salinity fields for the layer 5–50 m in 2013 (a) and 2014 (b); actual salinity field for the layer 5–50 m in 2013 (c) (from AARI data), difference between actual salinity field and reconstructed one for 2013 (d); PIOMAS salinity field for 2013 (e) and difference between PIOMAS salinity field and reconstructed one for 2013 (f).

1965, 1970, 1975, 1980, 1985, 1990, 2007, 2009 and 2011) were reconstructed, using modeled values of the PCs. The years were chosen at approximately equal intervals in order to reflect the different stages of the salinity field evolution through all decades. The average error of reconstruction for the chosen fields was 18.4%. As the first three EOF modes describe 61% of the variability of the initial fields, the error obtained is less than the variance not covered by the first three EOFs. Thus, we have a system of regression equations (statistical model) that may skillfully reproduce long-term salinity anomalies. The rest of the surface-layer salinity variance captured by higher order EOFs (∼39%) is likely explained by short-term and probably local processes such as ice

formation and cascading in polynya regions (Ivanov and Watanabe, 2013), deep convection or mixing with the AW upper boundary (Ivanov and others, 2012).

Thus, we have identified various patterns in Arctic Ocean surface-layer salinity fields using a reliable statistical model. In addition, we have found anomalies in the salinity fields which have occurred in the past, and conclude that more than 60% of surface-layer salinity variability is related to long-term processes ranging from water exchange with neighboring oceans (with periods longer than 20 years) to interannual variations of atmospheric circulation, ice pack characteristics (such as ice extent and volume export) and river runoff. The other nearly 40% is due to short-term and

local processes, such as changes in polynya activity or local mixing processes. Our findings again raise questions about non-linearities in global ocean circulation, particularly in the Arctic Ocean, which is strongly connected with Earth's climate system. In the future, information obtained about these anomalies may be helpful in determining whether Arctic Ocean salinity, and related oceanographic phenomena, have reached a critical threshold.

REFERENCES

Beszczynska-Möller A, Fahrbach E, Schauer U and Hansen E (2012) Variability in Atlantic water temperature and transport at the entrance to the Arctic Ocean, 1997–2010. *ICES J. Mar. Sci.*, **69**(5), 852–863 (doi: 10.1093/icesjms/fss056)

Borzelli G and Ligi R (1998) Empirical orthogonal function analysis of SST image series: a physical interpretation. *J. Atmos. Ocean. Technol*. **16**, 682–690

Bourgain P and Gascard JC (2012) The Atlantic and summer Pacific waters variability in the Arctic Ocean from 1997 to 2008. *Geophys. Res. Lett.*, **39**, L05603 (doi: 10.1029/2012GL051045)

Carmack EC (2000) The Arctic Ocean's freshwater budget: sources, storage and export. In Lewis EL, Jones EP, Lemke P, Prowse TD, Wadhams P eds. *The freshwater budget of the Arctic Ocean*. NATO Science Series (Series 2. Environment Security), **70**, Springer, Dordrecht, 91–126

Cronin MF and Sprintall J (2009) Wind and buoyancy-forced upper Ocean. In Steele J, Thorpe S, Turekian K eds. *Elements of Physical Oceanography: A derivative of the Encyclopedia of Ocean Sciences*, 237–245

Dickson B (1999) Oceanography: all change in the Arctic. *Nature*, **397**(6718), 389–391

Dima M and Lohmann G (2007) A hemispheric mechanism for the Atlantic multidecadal oscillation. *J. Clim.*, **20**, 2706–2719 (doi: 10.1175/JCLI4174.1)

Enfield DB, Mestas-Nunez AM and Trimble PJ (2001) The Atlantic multidecadal oscillation and its relationship to rainfall and river flows in the continental U.S. *Geophys. Res. Lett.*, **28**, 2077–2080

Gelderloos R, Straneo F and Katsman CA (2012) Mechanisms behind the temporary shutdown of deep convection in the Labrador Sea: lessons from the great salinity anomaly years 1968–71. *J. Clim.*, **25**, 6743–6755 (doi. org:10.1175/JCLI-D-11-00549.1)

Haak H, Jungclaus J, Mikolajewicz U and Latif M (2003) Formation and propagation of great salinity anomalies. *Geophys. Res. Lett.*, **30**, 1473 (doi: 10.1029/2003GL017065.9)

Hall A and Stouffer RJ (2001) An abrupt climate event in a coupled ocean-atmosphere simulation without external forcing. *Nature*, **409**(6817), 171

Hannachi A, Jolliffe IT and Stephenson DB (2007) Empirical orthogonal functions and related techniques in atmospheric science: a review. *Int. J. Climatol.*, **27**, 1119–1152 (doi: 10.1002/joc.1499)

Hill T and Lewicki P (2007) *Statistics: methods and applications*. StatSoft, Tulsa, OK

Ivanov V and Watanabe E (2013) Does Arctic sea ice reduction foster shelf-basin exchange? *Ecol. Appl.*, **23**(8), 1765–1777

Ivanov V, Alexseev V, Repina I, Koldunov N and Smirnov A (2012) Tracing Atlantic waters signature in the Arctic sea ice cover East of Svalbard. *Adv. Meteorol.*, **2012** (doi: 10.1155/2012/201818)

Jackson JM, Williams WJ and Carmack EC (2012) Winter sea-ice melt in the Canada Basin, Arctic Ocean. *Geophys. Res. Lett.*, **39**, L03603 (doi: 10.1029/2011GL050219)

Jahn A and 14 others (2012) Arctic Ocean freshwater: how robust are model simulations. *J. Geophys. Res. Oceans*, **117**(C8), 2156–2202 (doi: 10.1029/2012JC007907)

Karcher M and Oberhuber JM (2002) Pathways and modification of the upper and intermediate waters of the Arctic Ocean. *J. Geophys. Res.*, **107** (C6) (doi: 10.1029/2000JC000530)

Karcher M, Kauker F, Gerdes R, Hunke E and Zhang J (2007) On the dynamics of Atlantic water circulation in the Arctic Ocean. *J. Geophys. Res.*, **112**, C04S02 (doi: 10.1029/2006JC003630)

Komuro Y (2014) The impact of surface mixing on the Arctic river water distribution and stratification in a global ice–ocean model. *J. Clim.*, **27**, 4359–4370 (doi: 10.1175/JCLI-D-13-00090.1)

Korhonen M, Rudels B, Marnela M, Wisotzki A and Zhao J (2013) Time and space variability of freshwater content, heat content and seasonal ice melt in the Arctic Ocean from 1991 to 2011. *Ocean Sci.*, **9**(6), 1015–1055

Lebedev NV, Karpy VYU, Pokrovsky OM, Sokolov VT and Timokhov LA (2008) Specialized data base for temperature and salinity of the Arctic Basin and marginal seas in winter (in Russian). *Trudy AANII*, **448**, 5–17

Lindsay RW and Zhang J (2006) Assimilation of ice concentration in an ice-ocean model. *J. Atmos. Ocean. Technol.*, **23**, 742–749

Lique C, Treguier A, Scheinert M and Penduff T (2009) A model-based study of ice and freshwater transport variability along both sides of Greenland. *Clim. Dyn.*, **33**, 685–705 (doi: 10.1007/s0038200805107)

Macdonald RW, Harner T and Fyfe J (2005) Recent climate change in the Arctic and its impact on contaminant pathways and interpretation of temporal trend data. *Sci. Total Environ.*, **342**(1–3), 5–86, ISSN 0048–9697 (doi: 10.1016/j.scitotenv.2004.12.059)

Morison J and Smith JD (1981) Seasonal variations in the upper Arctic Ocean as observed at T-3. *Geophys. Res. Lett.*, **8**(7), 753–756 (doi: 10.1029/GL008i007p00753)

Morison J, Aagaard K and Steele M (2000) Recent environmental changes in the Arctic: a review. *Arctic*, **53**(4), 359–371

Morison J and 6 others (2012) Changing Arctic Ocean freshwater pathways. *Nature*, **481**, 66–70 (doi: 10.1038/nature10705)

Nguyen AT, Menemenlis D and Kwok R (2009) Improved modeling of the Arctic halocline with a subgrid-scale brine rejection

parameterization. *J. Geophys. Res.*, **114**, C11014 (doi: 10.1029/2008JC005121)

North GR, Bell TL, Cahalan RF and Moeng FJ (1982) Sampling errors in the estimation of empirical orthogonal functions. *Mon. Weather Rev.*, **10**, 699–706

Overland JE and Wang M (2010) Large-scale atmospheric circulation changes are associated with the recent loss of Arctic sea ice. *Tellus*, **62A**, 1–9

Pokrovsky OM and Timokhov LA (2002) The reconstruction of the winter fields of the water temperature and salinity in the Arctic Ocean. *Oceanology*, **42**, 822–830

Polyakov IV and 9 others (2008) Arctic Ocean freshwater changes over the past 100 years and their causes. *J. Clim.*, **21**, 364–384 (doi: 10.1175/2007JCLI1748.1)

Polyakov IV and 17 others (2010) Arctic Ocean warming contributes to reduced Polar Ice Cap. *J. Phys. Oceanogr.*, **40**, 2743–2756

Proshutinsky AY and Johnson MA (1997) Two circulation regimes of the wind-driven Arctic Ocean. *J. Geophys. Res.*, **102**, 12493–12514

Proshutinsky AY and 9 others (2009) Beaufort Gyre freshwater reservoir: state and variability from observations. *J. Geophys. Res.*, **114** (doi: 10.1029/2008JC005104)

Rabe B and 8 others (2011) An assessment of Arctic Ocean freshwater content changes from the 1990s to the 2006–2008 period. *Deep Sea Res. Part I*, **58**, 173–185

Rigor IG, Wallace JM and Colony RL (2002) Response of sea ice to the Arctic oscillation. *J. Clim.*, **15**, 2648–2663

Rudels B, Anderson LG and Jones EP (1996) Formation and evolution of the surface mixed layer and halocline of the Arctic Ocean. *J. Geophys. Res.*, **101**, 8807–8821

Rudels B, Jones EP, Schauer U and Eriksson P (2004) Atlantic sources of the Arctic Ocean surface and halocline waters. *Polar Res.*, **23**(2)

Schlosser P, Bauch D, Fairbanks R and Bönisch G (1994). Arctic river runoff: mean residence time on the shelves and in the halocline. *Deep Sea Res.*, Part I, **41**, 1053–1068

Shimada K and 7 others (2006) Pacific Ocean inflow: influence on catastrophic reduction of sea ice cover in the Arctic Ocean. *Geophys. Res. Lett.*, **33**, L08605 (doi: 10.1029/2005GL025624.)

Steele M and Boyd T (1998) Retreat of the cold halocline layer in the Arctic Ocean. *J. Geophys. Res.*, **103** (doi: 10.1029/98JC00580)

Steele M and 9 others (2001) Adrift in the Beaufort Gyre: a model intercomparison. *Geophys. Res. Lett.*, **28**, 2835–2838

Stigebrandt A (1984) The north pacific: a global-scale estuary. *J. Phys. Oceanogr.*, **14**, 462–470

Thompson DWJ and Wallace JM (1998) Observed linkages between Eurasian surface air temperature, the North Atlantic oscillation, Arctic sea-level pressure and the stratospheric polar vortex. *Geophys. Res. Lett.*, **25**, 1297–1300

Timmermans M-L (2015) The impact of stored solar heat on Arctic sea ice growth. *Geophys. Res. Lett.*, **42**, 6399–6406 (doi: 10.1002/2015GL064541)

Timmermans M-L and 6 others (2011) Surface freshening in the Arctic Ocean's Eurasian Basin: an apparent consequence of recent change in the wind-driven circulation. *J. Geophys. Res.*, **116** (doi: 10.1029/2011JC006975)

Timokhov LA and Tanis F (1997) *Environmental working group Joint U.S.-Russian Atlas of the Arctic Ocean*. National Snow and Ice Data Center, Boulder, Colorado, USA, (http://dx.doi.org/10.7265/N5H12ZX4)

Timokhov LA, Chernyavskaya EA, Nikiforov EG, Polyakov IV and Karpy VYu (2012) Statistical model of inter-annual variability of the Arctic Ocean surface layer salinity in winter (in Russian). *Probl. Arkt. Antarkt.*, **91**, 89–102

Toole JM and 5 others (2010) Influences of the ocean surface mixed layer and thermohaline stratification on Arctic sea ice in the central Canada Basin. *J. Geophys. Res.*, **115**, C10018 (doi: 10.1029/2009JC005660)

Trenberth KE and Hurrell JW (1994) Decadal atmosphere-ocean variations in the Pacific. *Clim. Dyn.* **9**, 303–319

Treshnikov AF (1959) Arctic Ocean surface waters (in Russian). *Probl. Arkt.*, **7**, 5–14

Walin G (1985) The thermohaline circulation and the control of ice ages. *Palaeogeogr. Palaeoclimatol. Palaeoecol.*, **50**(2–3), 323–332, ISSN 0031-0182 (doi: 10.1016/0031-0182(85)90075-6)

Wang J and 7 others (2009) Is the dipole anomaly a major driver to record lows in Arctic summer sea ice extent? *Geophys. Res. Lett.*, **36**, L05706 (doi: 10.1029/08GL036706)

Weyl PK (1968) The role of the oceans in climatic change: a theory of the Ice ages. In Mitchell JM eds. *Causes of climatic change*. Meteorological Monographs, 8, American Meteorological Society, Boston, MA, 37–62

Woodgate RA, Weingartner T and Lindsay R (2010) The 2007 Bering strait oceanic heat flux and anomalous Arctic sea-ice retreat. *Geophys. Res. Lett.*, **37**, L01602 (doi: 10.1029/2009GL041621)

Wu B, Wang J and Walsh JE (2006) Dipole anomaly in the winter Arctic atmosphere and its association with sea ice motion. *J. Clim.*, **19**, 210–225

Zhang J and Rothrock DA (2003) Modeling global sea ice with a thickness and enthalpy distribution model in generalized curvilinear coordinates. *Mon. Weather Rev.*, **131**(5), 681–697.

Zhang J, Woodgate R and Moritz R (2010) Sea ice response to atmospheric and oceanic forcing in the Bering Sea. *J. Phys. Oceanogr.*, **40**, 1729–1747 (doi: 10.1175/2010JPO4323.1)

APPENDIX
DATA AND OBSERVATION DENSITY

THE EMPIRICAL EQUATIONS FOR THE FIRST THREE PRINCIPAL COMPONENTS

The equations are derived from the formula for multiple linear regression

$$y_i = \sum a_{ij} x_{ij} + b_i, \tag{A1}$$

where the y_i are the principal components (PCs) PC_i; the x_{ij} are the variables independent of the y_i (the different environmental factors), the a_{ij} are the regression coefficients and the b_i are the intercepts. To determine which predictors to include in each regression model, we used the 'forward stepwise' method. Each predictor leads the salinity empirical orthogonal function (EOF) by some number of years, and these temporal lags were determined to maximize the variance accounted for by each predictor.

The values of the correlation coefficients (R), coefficients of determination (R^2) and F-criteria (Hill and Lewicki, 2007) are presented in Table A2. The values of all F-criteria exceed the threshold indicating that the models are statistically significant. The correlation coefficients for all PCs were statistically significant and varied from 0.55 (R_3) to 0.88 (R_1).

Table A1. Datasets used for reconstruction and gridding of surface-layer salinity fields

Expedition (cruise) or code of expedition (cruise)	Regions, water areas	Date of station performance First	Number of stations Last	
SEVER05	ArB, ChS, EsS	03/31/1950	04/02/1951	51
Toros1951	KrS, LpS	04/08/1951	04/24/1951	9
SEVER07	ArB, KrS, LpS	04/16/1955	05/15/1955	105
NP05	ArB	05/20/1955	03/20/1956	14
SEVER08	ArB, ChS, EsS	04/04/1956	05/16/1956	48
SEVER09	ArB	03/1957	05/1957	11
Lena1958	GrS	03/11/1958	03/25/1958	28
SEVER10	ArB	03/1958	06/1958	18
WOD98_31_3272	ArB	03/29/1958	04/14/1958	3
SEVER11	ArB	03/1959	05/1959	30
Storm1959	GrS	04/26/1959	06/12/1959	59
NP08	ArB	06/30/1959	02/15/1962	52
SEVER12	ArB	03/1960	05/1960	27
WOD98_18_11445	ArB	04/18/1960	05/30/1960	6
WOD98_31_672	ArB	12/29/1960	12/29/1960	1
SEVER13	ArB	03/1961	05/1961	27
SEVER14	ArB	03/1962	05/1962	29
SEVER15	ArB	02/1963	05/1963	58
SEVER16	ArB, ChS, EsS, KrS, LpS	03/23/1964	05/13/1964	43
SEVER17	ArB, ChS, EsS, KrS, LpS	03/17/1965	05/11/1965	44
NP14	ChS, EsS	05/30/1965	01/24/1966	16
SEVER18	ArB, ChS, EsS, KrS, LpS	03/12/1966	05/07/1966	42
SEVER19	ArB, ChS, EsS, KrS, LpS	03/19/1967	04/26/1967	32
OBTAZ1967	KrS	04/06/1967	08/21/1967	26
NP15	ArB	04/30/1967	03/14/1968	18
SEVER20	ArB, ChS, EsS, KrS, LpS	03/19/1968	05/03/1968	60
WOD98_31_2170	ArB	03/29/1968	04/06/1968	3
AUGMS1968	KrS	04/09/1968	05/03/1968	45
NP17	ArB	06/25/1968	09/26/1969	45
SEVER21	ArB, ChS, EsS, KrS, LpS	03/18/1969	05/14/1969	95
NP16	ArB	04/22/1969	03/15/1972	83
Tiksi1969	LpS	04/25/1969	12/08/1969	51
DUGMS1970	KrS	01/06/1970	12/18/1970	73
SEVER22	ArB, ChS, EsS, KrS, LpS	03/30/1970	05/11/1970	90
AUGMS1970	KrS	04/12/1970	05/01/1970	70
NP18	ArB	05/19/1970	03/15/1971	20
NP20	ArB, EsS	05/20/1970	04/15/1972	49
NP19	ArB, EsS	11/14/1970	03/26/1973	43
DUGMS1971	KrS	01/07/1971	12/23/1971	73
Tiksi1971	LpS	01/10/1971	11/30/1971	106
SEVER23	ArB, ChS, EsS, KrS, LpS	02/28/1971	05/10/1971	81
AUGMS1971	KrS	04/19/1971	08/07/1971	112
DUGMS1972	KrS	01/06/1972	12/27/1972	95
Tiksi1972	LpS	01/10/1972	06/20/1972	54
SEVER24	ArB, ChS, EsS, KrS, LpS	02/29/1972	05/07/1972	51
AUGMS1972	KrS	04/20/1972	05/30/1972	80
NP21	ArB, EsS	05/30/1972	03/21/1974	30
SEVER25	ArB, BfS, ChS, EsS, KrS, LpS	03/19/1973	05/10/1973	178
Liman1973	KrS, ObR	03/20/1973	09/23/1973	18
Tiksi1973	LpS	05/04/1973	11/16/1973	109
Tiksi1974	LpS	12/14/1973	12/15/1974	119
DUGMS1974	KrS	01/08/1974	12/27/1974	62
SEVER26	ArB, BfS, ChS, EsS, KrS, LpS	03/11/1974	05/10/1974	166
NP22	ArB, BfS, ChS, EsS	03/23/1974	03/03/1982	117
DUGMS1975	KrS	01/04/1975	09/23/1975	145
Tiksi1975	LpS	01/15/1975	12/15/1975	55
SEVER27	ArB, BfS, ChS, EsS, GrS, KrS, LpS	03/13/1975	04/30/1975	188
DUGMS1976	KrS	01/07/1976	12/16/1977	312
AUGMS1976	KrS, ObR	02/24/1976	09/24/1976	249
SEVER28	ArB, BfS, ChS, EsS, GrS, KrS, LpS	03/11/1976	05/09/1976	155
NP23	ArB, EsS	05/30/1976	10/17/1978	83
SEVER29	ArB, BfS, ChS, EsS, KrS, LpS	03/01/1977	04/29/1977	150
AUGMS1977	KrS, ObR	03/03/1977	05/27/1977	101
WOD98_31_10614	BeS	03/31/1977	04/03/1977	16
VegaDUGMS1978	KrS	01/19/1978	12/22/1978	10
SEVER30	ArB, BaS, ChS, EsS, KrS, LpS	03/08/1978	05/10/1978	185
WOD98_31_13021	BfS	04/04/1978	07/29/1978	46
NP24	ArB	12/19/1978	09/30/1980	31

Table A1. (*Cont.*)

Expedition (cruise) or code of expedition (cruise)	Regions, water areas	Date of station performance First	Last	Number of stations
VegaDUGMS1979	KrS	01/09/1979	11/21/1979	22
SEVER31	ArB, BaS, BfS, ChS, EsS, GrS, KrS, LpS	03/02/1979	05/19/1979	205
WOD98_18_8924	BeS, ChS	04/19/1979	04/28/1979	8
VegaDUGMS1980	KrS	01/17/1980	09/26/1980	17
SEVER32	ArB, BaS, ChS, EsS, KrS, LpS	02/15/1980	05/15/1980	138
WOD98_31_10726	BfS	03/05/1980	07/02/1980	62
VegaDUGMS1981	KrS	01/06/1981	12/23/1981	32
DUGMS1981	KrS	03/17/1981	10/01/1981	344
SEVER33	ArB, ChS, EsS, KrS, LpS	03/18/1981	05/18/1981	112
VegaDUGMS1982	KrS	01/06/1982	12/29/1982	14
SEVER34	ArB, ChS, EsS, KrS, LpS	02/17/1982	05/19/1982	117
DUGMS1982	KrS	03/20/1982	05/07/1982	155
AUGMS1982	KrS	03/27/1982	06/07/1982	190
NP25	ArB	05/27/1982	03/11/1984	25
VegaDUGMS1983	KrS	01/05/1983	12/06/1983	20
SEVER35	ArB, ChS, EsS, KrS, LpS	02/25/1983	05/14/1983	235
DUGMS1983	KrS	03/22/1983	05/02/1983	67
NP26	ArB	07/01/1983	02/21/1986	35
VegaDUGMS1984	KrS	01/05/1984	11/26/1984	24
AUGMS1984	KrS	01/06/1984	12/24/1984	175
TUGKS1984	LpS	01/15/1984	12/27/1984	112
SEVER36	ArB, ChS, EsS, KrS, LpS	02/27/1984	05/13/1984	247
TUGMS1984	EsS, LpS	03/23/1984	05/22/1984	20
DUGMS1984	KrS	04/01/1984	05/18/1984	36
Pevek1984	EsS	04/10/1984	12/29/1984	37
NP27	ArB, EsS	06/26/1984	03/10/1987	35
TUGKS1985	EsS, LpS	01/03/1985	09/24/1985	213
VegaDUGMS1985	KrS	01/03/1985	12/24/1985	20
Pevek1985	EsS	01/10/1985	03/29/1985	17
SEVER37	ArB, ChS, EsS, KrS, LpS	02/25/1985	05/10/1985	296
TUGMS1985	EsS, LpS	03/21/1985	05/04/1985	39
WOD98_31_12556	BfS	04/01/1985	04/18/1985	7
DUGMS1985	KrS	04/02/1985	09/20/1985	209
AUGMS1985	KrS	04/05/1985	07/01/1985	38
VegaDUGMS1986	KrS	01/06/1986	12/26/1986	22
SEVER38	ArB, ChS, EsS, KrS, LpS	02/26/1986	06/06/1986	196
DUGMS1986	KrS	04/03/1986	08/24/1986	96
SEVER39	ArB, ChS, EsS, KrS, LpS	02/25/1987	06/08/1987	284
NP28	ArB, GrS	05/07/1987	01/17/1989	34
SEVER40	ArB, BeS, ChS, EsS, LpS	03/09/1988	05/19/1988	282
AUGE1988	HtR, LpS	05/06/1988	09/19/1988	100
SEVER41	ArB, BeS, ChS, EsS, LpS	02/27/1989	06/02/1989	262
NP31	ArB, BfS	06/29/1989	03/26/1990	10
SEVER42	BeS, ChS, EsS	01/19/1990	08/11/1990	150
SEVER43	KrS	04/25/1991	05/24/1991	20
SEVER44	ArB, BeS, ChS, EsS, LpS	02/27/1992	06/02/1992	206
SEVER45	BaS, KrS, WhS	04/08/1993	06/14/1993	180
CELTIC VOYAGER	NoS	04/07/2007	04/07/2007	1
CLUPEA	NoS	05/10/2007	05/12/2007	57
LLZG (G.O. SARS)	NoS, BaS	02/07/2007	11/26/2009	350
HAKON MOSBY	NoS, GrS	01/10/2007	12/05/2009	989
HERWIG, W. (JAN.73)	NoS	02/07/2007	01/10/2007	14
ITP01	Bfs	01/01/2007	01/08/2007	32
ITP04	ArB	01/01/2007	05/31/2007	302
ITP05	ArB	01/01/2007	05/31/2007	453
ITP06	ArB	01/01/2007	05/31/2008	580
ITP07	ArB	04/28/2007	11/01/2007	134
LDGJ (JOHAN HJORT)	BaS, GrS, NoS	01/15/2007	12/04/2009	1178
MAGNUS HEINASON (OW2252)	NoS	02/15/2007	11/10/2008	364
Transarctica_2007	ArB, LpS, KrS	05/15/2007	05/31/2007	49
SCOTIA	NoS	01/29/2007	02/14/2010	288
Tara	ArB	01/13/2007	12/10/2007	35
Twin Otter	ArB	04/21/2007	05/07/2007	10
CELTIC EXPLORER	NoS	05/21/2008	05/21/2008	3
TRANSDRIFT XIII (Polynya)	LpS	04/10/2008	05/05/2008	17
ITP08	ArB	01/01/2008	05/31/2008	303
ITP09	ArB	01/01/2008	02/27/2009	408

Table A1. (*Cont.*)

Expedition (cruise) or code of expedition (cruise)	Regions, water areas	Date of station performance First	Number of stations Last	
ITP10	ArB	01/01/2008	05/25/2008	293
ITP11	ArB	01/01/2008	05/31/2009	630
ITP13	ArB	01/01/2008	05/31/2008	317
ITP16	ArB	01/01/2008	04/03/2008	140
ITP18	BrS	01/01/2008	05/31/2008	317
ITP19	ArB, GrS	04/08/2008	11/21/2008	216
LAHV (JAN MAYEN)	BaS	02/07/2008	03/06/2009	304
NP35	ArB	01/01/2008	12/31/2008	152
NPEO_2008 (Twin Otter)	ArB, BfS	03/21/2008	04/20/2008	43
TRANSDRIFT XV (Polynya)	LpS	03/24/2009	04/23/2009	15
HERWIG, W. (JAN.73)	NoS	02/10/2009	02/15/2009	16
NP36	ArB	01/01/2009	12/31/2009	151
ITP21	ArB	01/01/2009	05/31/2009	288
ITP23	ArB	01/01/2009	05/31/2010	599
ITP24	ArB	01/01/2009	05/31/2009	299
ITP25	ArB	01/01/2009	05/31/2009	298
ITP26	ArB	01/01/2009	02/26/2009	114
ITP27	ArB	01/01/2009	01/20/2009	40
ITP29	ArB	01/01/2009	05/31/2010	589
ITP33	BfS, ArB	01/01/2010	01/25/2011	351
ITP34	BfS, ArB	01/01/2010	05/31/2010	298
ITP37	ArB	01/01/2010	12/24/2010	301
ITP38	ArB, GrS	04/19/2010	12/28/2010	170
NP37	ArB	01/01/2010	12/30/2010	112
NPEO_2010 (Hercules)	BfS	05/25/2010	05/26/2010	4
NPEO_2011(Twin Otter)	ArB	04/28/2011	05/08/2011	25
ITP41	ArB	01/01/2011	05/31/2012	607
ITP42	BfS, ArB	01/01/2011	04/15/2011	201
ITP43	BfS	01/01/2011	02/11/2011	83
ITP47	ArB	04/11/2011	02/28/2012	434
PALEX 2011	ArB	04/10/2011	04/20/2011	20
NP38	ArB	01/01/2011	11/01/2011	147
BARNEO2012	ArB	04/06/2012	04/17/2012	24
ITP48	ArB	01/01/2012	11/16/2012	446
ITP53	BfS	01/01/2012	05/31/2012	304
ITP55	ChS	01/01/2012	05/08/2012	257
ITP56	ArB, GrS	04/15/2012	12/31/2012	185
ITP63	ArB	04/21/2012	12/31/2012	161
NP39	ArB	01/01/2012	12/31/2012	143
SWITCHYARD2012	ArB, NrS	05/03/2012	05/21/2012	23
TRANSDRIFT XX	LpS	03/26/2012	04/19/2012	7
All expeditions	All regions	03/31/1950	12/31/2012	24 557

Conventional names of regions and water areas in column 2: ArB, Arctic Basin; BaS, Barents Sea; BeS, Bering Sea; BfS, Beaufort Sea; ChS, Chukchi Sea; EsS, East Siberian Sea; GrS, Greenland Sea; HtR, Khatanga river mouth zone; JpS, Japan Sea; KrS, Kara Sea; LpS, Laptev Sea; NoS, Norwegian Sea; NrS, Nares Strait; ObR, Ob estuary zone; WhS, White Sea.
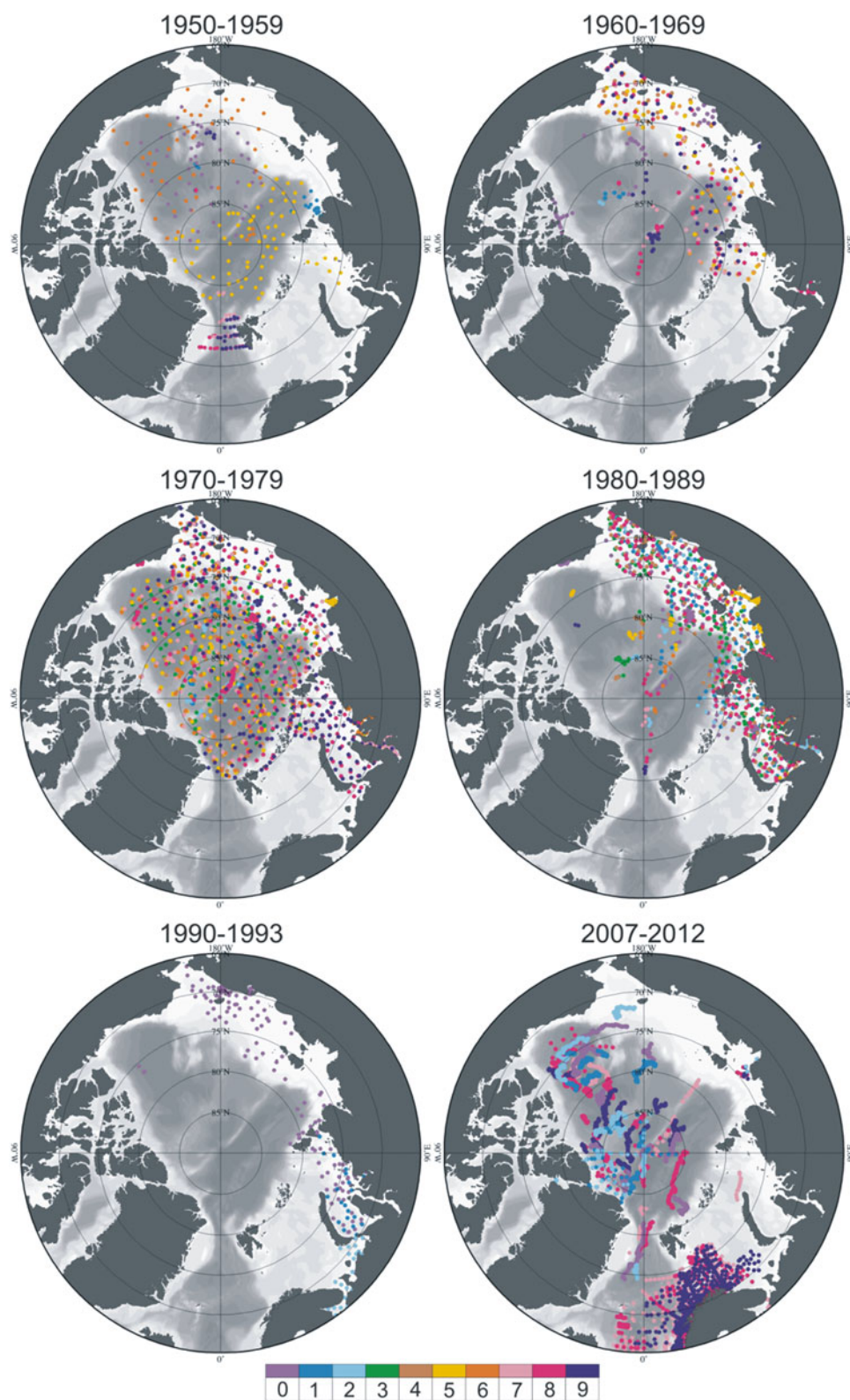
1950-1959 **1960-1969**

1970-1979 **1980-1989**

1990-1993 **2007-2012**

0 1 2 3 4 5 6 7 8 9

Fig. A1. Observation density. Color bar indicates the last number of the year in each decade. The total number of observations in the 1950s – 428, 1960s – 751, 1970s – 3837, 1980s – 4374, 1990s – 556, 2000s – 14691.
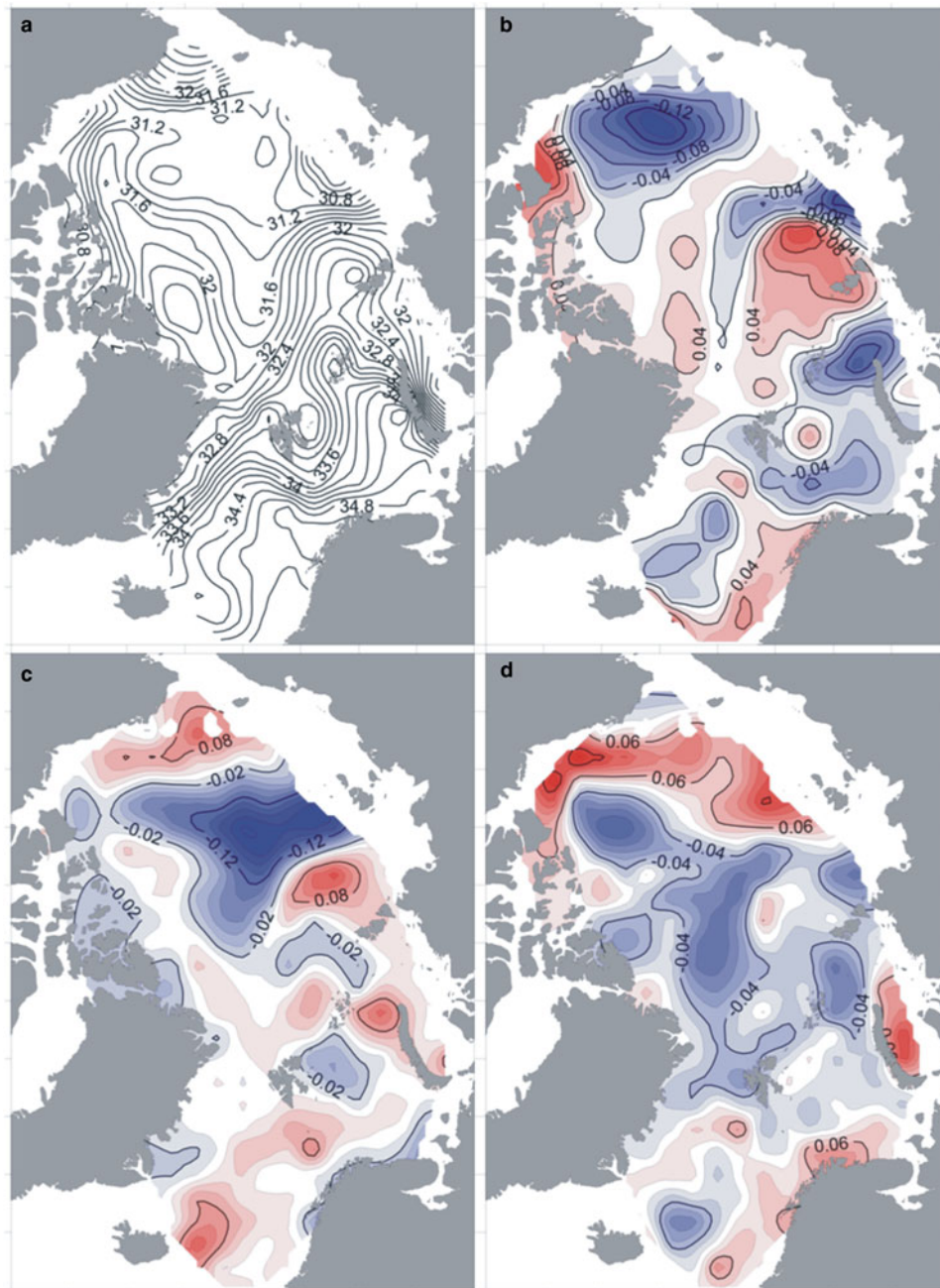
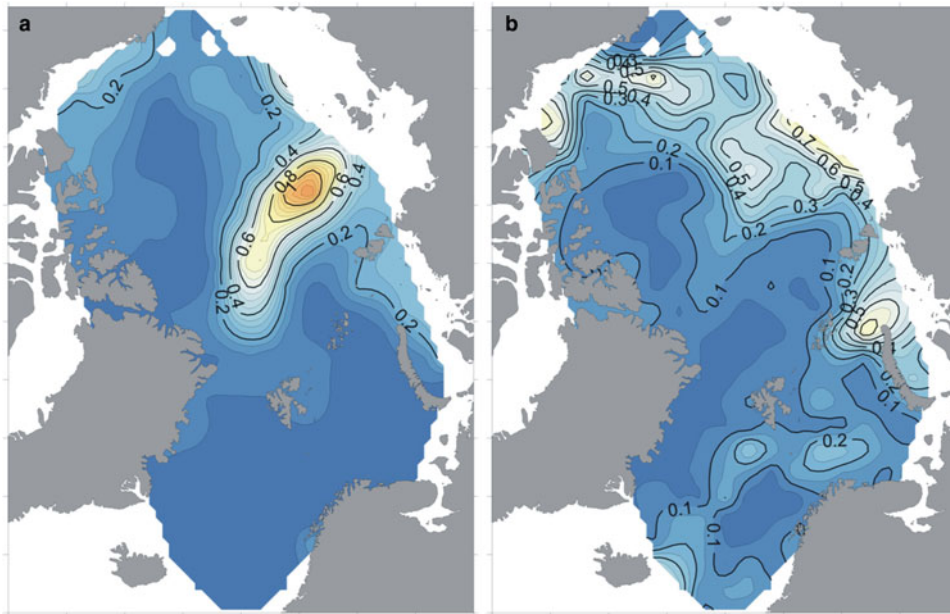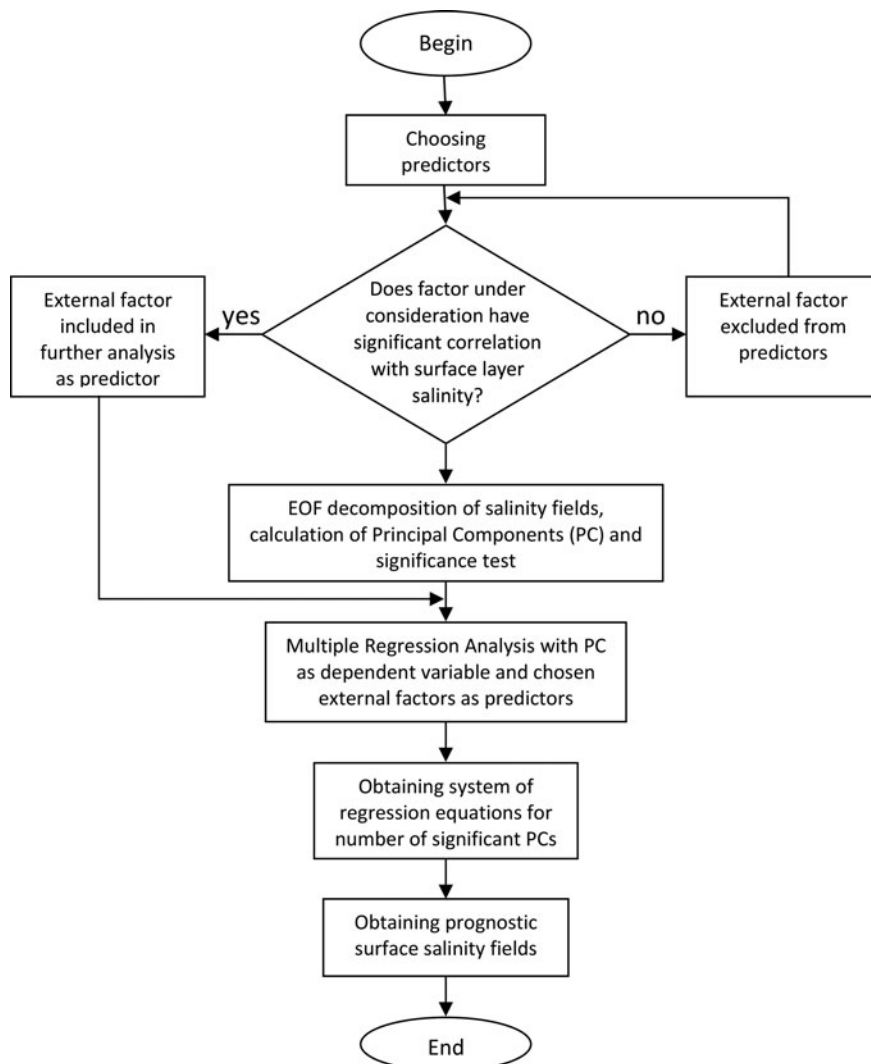**Fig. A2.** Same as Figure 2, but for salinity averaged annually over the upper 50 m of PIOMAS data for 1978–2012.

Fig. A3. Variance maps of surface-layer salinity for the 1978–2012 period: (a) AARI database, (b) PIOMAS data.

Box. 1. Schematic diagram of the conceptual statistical model.

Table A2. The empirical statistical model developed for each of the first three PCs. The lower case indicates the months of an averaging period or the first letters of the sea name (see Table 1)

PC_i	Statistical equations	Multiple R	Multiple R^2	Adjusted R^2	F-criteria
PC_1	$PC_1 = 11.60 \times AMO(-7)^* + 0.008 \times OW_{EC}(-1) + 1.28 \times PDO$ $(-10) + 1.86 \times AO_{VII\ -IX}(-1) - 7.87$	0.88	0.78	0.76	40.07 (4;45)[†]
PC_2	$PC_2 = -1.28 \times AO_{VII\ -IX}(-1) + 1.22 \times AD_{VII\ -IX}(-1) - 1.18 \times$ $PDO(-6) + 0.008 \times RIV_{LEC}(-4) - 8.07$	0.73	0.53	0.49	12.81 (4;45)
PC_3	$PC_3 = -0.97 \times AD_{X\ -III}(-1) - 4.00 \times AMO(-10) - 0.68 \times$ $PDO(-3) + 0.004 \times RIV_{LEC}(-5) - 4.82$	0.55	0.30	0.23	4.76 (4;45)

* Time shift for every predictor is indicated in parentheses (minus means that predictor leads the dependent variable).
† Numbers of degrees of freedom are indicated in parentheses.